Nano Research 2018, 11(6): 3175–3181
https://doi.org/10.1007/s12274-017-1723-z
Research Article
ISSN 1998-0124
CN 11-5974/O4

Three-dimensional macroscale assembly of Pd nanoclusters

Kai Wang, Haifeng Lin, Bing Ni, Haoyi Li, Muhammad Aurang Zeb Gul Sial, Haozhou Yang, Jing Zhuang, and Xun Wang (✉)

Key Lab of Organic Optoelectronics and Molecular Engineering, Department of Chemistry, Tsinghua University, Beijing 100084, China

Received: 27 April 2017
Revised: 2 June 2017
Accepted: 10 June 2017

KEYWORDS
nanocluster,
macroscale assembly,
honey comb structure,
porous material

ABSTRACT

Construction of macro-materials with highly oriented microstructures and well-connected interfaces between building blocks is significant for a variety of applications. However, it is still challenging to confine the desired structures. Thus, well-defined building blocks would be crucial to address this issue. Herein, we present a facile process based on 1.8 nm Pd nanoclusters (NCs) to achieve centimeter-size assemblages with aligned honeycomb structures, where the diameter of a single tubular moiety is ~ 4 μm. Layered and disordered porous assemblages were also obtained by modulating the temperature in this system. The reconciled interactions between the NCs were crucial to the assemblages. As a comparison, 14 nm Pd nanoparticles formed only aggregates. This work highlights the approach of confining the size of the building blocks in order to better control the assembly process and improve the stability of the structures.

1 Introduction

The construction of macro-materials with well-aligned microstructures is of profound importance to maximize the advantages offered by nanomaterials. However, it is essentially difficult to confine the desired structures. Macro-materials with highly oriented micro- and meso-pores are significant for numerous applications in various research areas including biomimetics [1–3], virus selection [4], compressible materials [5–7], particles filtration [8], catalysis [9–11]. While uniform nanocrystals are used as building blocks for super-crystals [12, 13], the construction of macro-structures with highly oriented micro- and meso- pores is still a challenge. This is because large nanocrystals would weaken the interactions due to their ultrahigh weight, while the rigidity of the nanocrystals would limit the diversification of the assembly [14–16]. In recent years, the fabrication of aligned macro-materials has undergone rapid development in terms of synthetic techniques [1, 17, 18], solidification principles [19–22], functional realizations [23, 24], and even fabrication of complex composites [5–7]. Consequently, it is an essential and primary task to tap into the potential of these well-defined building blocks.

Recent studies have revealed that the size of the

Address correspondence to wangxun@mail.tsinghua.edu.cn

nanocrystals has a great impact on their properties as well as the interactions between them. Numerous novel phenomena based on the properties of nanocrystals and their interactions have been discovered, such as macromolecule-like viscosity in ultrathin nanowires [25, 26]; similarly, sub-nanometer In_2S_3 nanobelts have been observed to curl into uniform rolls and assemble into micro-size superlattice structures [27]. One-dimensional (1D) and two-dimensional (2D) sub-nanometer inorganic nanocrystals behave like polymers with flexible morphologies. Zero-dimensional (0D) nanoclusters can be regarded as a special class of molecules, and the energy needed to transform their morphology is almost of the same order as that of weak interactions. The weight of these molecules clearly does not weaken the interface [14]. Therefore, inorganic nanocrystals in the sub-nanometer scale would interact with each other almost in the same energy scale via interfaces. Additionally, a large inorganic component could easily overwhelm the interactions between the interfaces, resulting in instabilities such as aggregations. Based on the above, we believe that it is possible to construct well-aligned porous materials in the macro-scale based on ultra-small nanocrystals, by sophisticated control of the interactions between them.

Herein, we demonstrate a highly oriented honeycomb assemblage based on 1.8 nm Pd NCs (PNA1), via an accessible directional freeze casting process in combination with sol-gel synthesis, spanning multiple length scales from 0D sub-nanometer dots to 3D centimeter-size macroscopic structures. Meanwhile, the walls of the structures are 2D micrometer-size films. Other assemblages with layered and disordered porous morphologies were achieved by modulating the freezing conditions. The size effect in this system was studied in detail. There are two approaches that can be considered for the fabrication of assemblies, (i) building blocks with ultra-high speed that escape from the ice solidification front and assemble into the desired structures, (ii) the similarity in energy scale between ultra-small building blocks and their interactions. Finally, the fabricated assemblages were applied as heterogeneous catalysts for the reduction of p-nitrophenol and as hydrogen storage materials.

2 Experimental

To obtain highly oriented assemblages, we first prepared a homogeneous suspension of 1.8 nm Pd NCs as the raw material, followed by a directional freeze casting process (Fig. 1(a)), in combination with sol-gel synthesis. The water-soluble Pd NCs were synthesized by a solvothermal method (for details, see the Electronic Supplementary Material (ESM)). The transmission electron microscopy (TEM) image (Fig. 1(b)) and high-resolution TEM (HRTEM) image (inset in Fig. 1(b)) revealed the uniform and monodispersed Pd NCs with a diameter of 1.8 nm. The bulk sample (Fig. S1(a) in the ESM) was obtained after purifying and drying the synthesized Pd NCs. We considered that the ultra-small size of the Pd NCs weakened the rigidity of the inorganic structures and simultaneously strengthened the interactions, leading to a cross-linked structure instead of separate powders. Further studies

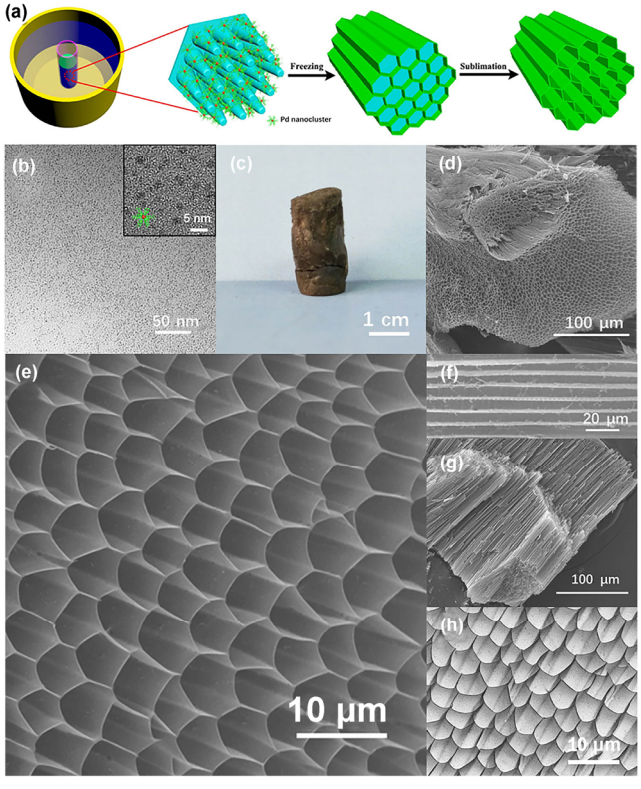

Figure 1 (a) Schematic representation of the synthesis of PNA1. (b) TEM image of the Pd NCs. (c) A digital photograph of PNA1. (d) and (e) SEM images of PNA1, (f) and (g) SEM images for side views of the open tubes and PNA1, respectively. (h) SETM image of PNA1. The inset in (b) shows the HRTEM image and a model of the Pd NCs.

revealed that gels (Fig. S1(b) in the ESM) were obtained upon soaking the bulk in proper amount of water. These Pd NC gels were found to be extraordinarily effective for the synthesis of highly oriented structures, after a liquid nitrogen bath for 5 min followed by sublimation of the ice by freeze drying (Fig. 1(a)).

3 Results and discussion

A photograph (Fig. 1(c)) and scanning electron microscopy (SEM) images (Figs. 1(d)–1(h)) displayed various aspects of PNA1. The assemblage resembled a container and maintained the cylindrical shape of the gel with a tiny shrinkage. Figure 1(d) shows a magnified view of the orientation of the pores; the walls of PNA1 were longer than hundreds of micrometers. These "channels" were all in the direction from the surface to the center of the assemblage (Fig. S1(c) in the ESM), which was along the ice growth route. An obvious step formed by pressing during the sample preparation for SEM and some bends revealed the flexibility of PNA1. Figure 1(e) clearly displays the honeycomb structure with regularly ranked pores, which were ~ 4 μm in diameter on average. Most of them were hexagons, and the thickness of the walls was about 60–80 nm (Fig. S2(a) in the ESM). Figures 1(f) and 1(g) show the side views of the open tubes and PNA1 respectively, revealing the parallel alignment of "channels" in a large area. As shown in Fig. 1(h), a different viewing angle of PNA1 was offered by scanning TEM (STEM). The walls of PNA1 were observed to be smooth with a small bunch of fragments, which correspond to the parts that did not assemble.

Other macroscale assemblages were also obtained by adjusting the freezing conditions. Macroscale layered assemblages based on Pd NCs (PNA2) were achieved by freezing the gel on a steel plate inserted on the surface of the liquid nitrogen for 10 min, which prevented direct contact, and thus slowed down the freezing speed. A schematic representation of this directional freeze casting process is provided in Fig. 2(a).

A slow freezing procedure for about 8 h in a refrigerator at ~ −4 ℃ yielded a macroscale disordered porous assemblage based on Pd NCs (PNA3). Figures 2(b)–2(d) and Figs. 2(e)–2(g) exhibit the

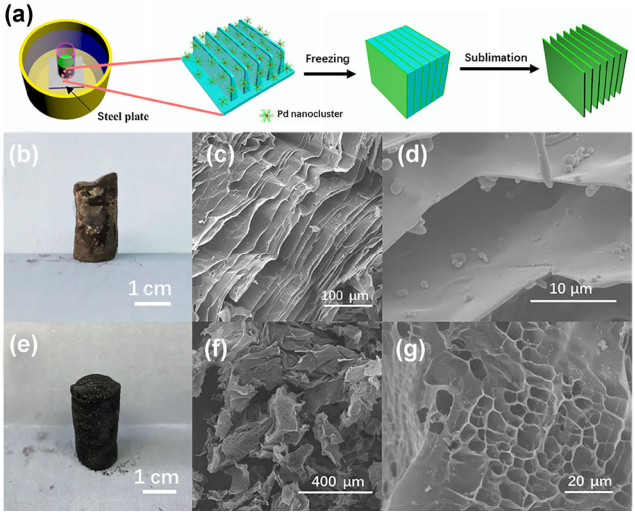

Figure 2 (a) Synthetic scheme of PNA2. (b) A photograph of PNA2. (c) and (d) SEM images of PNA2. (e) A photograph of PNA3. (f) and (g) SEM images of PNA3.

snapshots and SEM images of the PNA2 and PNA3 samples, respectively. PNA2 reveals an aligned structure with parallel layers, where the layer surface was very large, extending for hundreds of micrometers. The gaps between the layers were about tens of micrometers, and the thickness of each layer was less than 100 nm (Fig. S2(b) in the ESM). The pores in PNA3 exhibited a wide size distribution. Visually, the oriented structures of PNA1 and PNA2 were brown, while PNA3 was black. We conjectured that the ordered structure and micrometer thickness of the walls resulted in certain optical effects that were not present in the disordered structures, leading to the color change.

To further investigate the structures of the assemblages (Fig. 3 and Figs. S7–S10 in the ESM), mercury intrusion porosimetry was carried out to analyze the porosity and the pore size distribution. The bulk Pd NCs without assembly showed almost no porosity which conformed to intuitive observation. The PNA1, PNA2, and PNA3 samples had porous structures with porosity values of 77.4%, 65.4%, and 88.3%. The total pore volumes were 7.25, 6.07, and 8.23 mL/g for PNA1, PNA2, and PNA3, respectively. Moreover, the major peaks in the pore size distribution were seen at 2.08, 13.95, and 73.04 μm for PNA1, PNA2, and PNA3, respectively, which matched well with the structures. Deformation of the pores sometimes occurred in PNA1

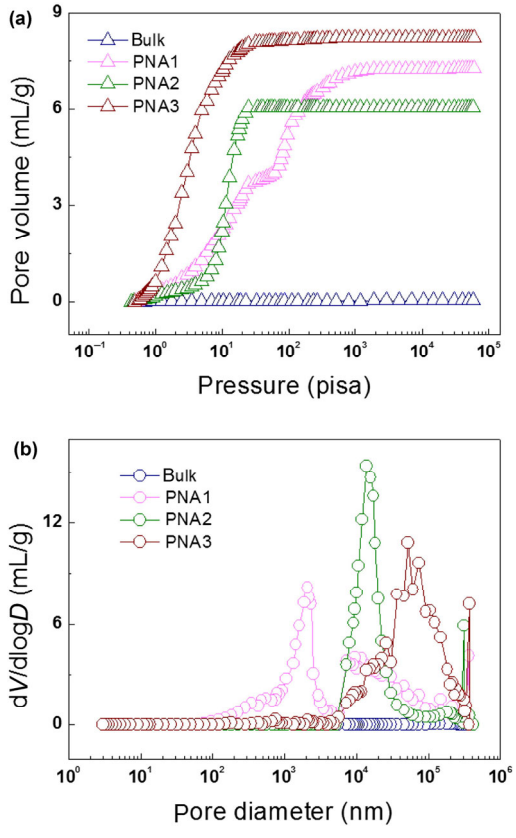

Figure 3 (a) Pressure–pore volume curve in the intrusion stage of mercury intrusion porosimetry. (b) Pore size distribution curves of PNA1, PNA2, PNA3 and the bulk counterpart.

and PNA2 (Figs. S3(a) and S3(b) in the ESM) due to exogenous impact, which made the results smaller than the SEM observations. The pore size distribution of PNA3 was broad, indicating the disorder of the pores.

Freezing conditions were critical for shaping the microstructures, which was accomplished by shaping the ice crystals at the nucleation stage and controlling the growth speed of the ice crystals [22]. The homogeneous nucleation of ice occurred at the initial stage near the cold surface, (circle surface of container for PNA1 and PNA3, bottom of container for PNA2), where the gels were placed for freeze casting. Then ice crystals grew along the freezing direction and in random directions. For PNA1, the freezing temperature was very low and the temperature gradient was very large. Thus, the growth of ice crystals in the freezing direction was much greater than in the randomly oriented directions, leading to the eventual formation of ice columns. While the temperature gradient for PNA2 was smaller than for PNA1, it was still large enough to ensure that the primary growth occurred in the freezing direction. Pseudo lamellar growth along the radial direction also occurred, leading to layered ice crystals. In the case of PNA3, the temperature was much higher, with no obvious temperature gradient. The growth of ice crystals continued for a long time, resulting in a final structure with no clear orientation. In addition, hexagonal ice is the most common structure of the 15 known crystalline phases of ice [28]. The temperature gradient along the *a* axis, perpendicular to the *c* axis, was kinetically favorable, which agreed with the results that hexagonal tubes were obtained in PNA1 and layered films in PNA2.

The size of the Pd nanocrystals was crucial for obtaining highly oriented assemblages. The 1.8 nm Pd NCs could get close to each other and finally formed 1D chains when introducing a little amount of poor solvent into reaction system. Upon the addition of water after a few minutes, the bulk Pd NCs separated to form films on the surface (Figs. 4(c) and 4(d)), pointing towards the strong interactions between the Pd NCs. The effect of the building block size was further investigated by carrying out contrastive experiments with PVP-coated Pd nanoparticles (NPs, average diameter of 14 nm, Fig. S4(a) in the ESM). The structures achieved were compared to those obtained for different sizes of Pd nanocrystals. The SEM images (Figs. 4(e) and 4(f)) revealed several micro spheres and some films without oriented structures formed by the freeze casting of Pd NPs. In the schemes representing the ice solidification front in both cases, the black arrows revealed the direction of ice growth. Learning from other similar systems [23, 28], we attempted to explain the growth mechanism observed herein. For Pd NCs or NPs close to the ice solidification front, the most important forces, repulsive force F_r and attractive drag force F_a, are given by the equations below

$$F_r = \pi D \Delta\sigma \left(\frac{a_0}{d}\right)^n \quad (1)$$

$$F_a = \frac{3\pi\eta v D^2}{2d} \quad (2)$$

Where d is the diameter of building blocks (1.8 nm for Pd NCs, 14 nm for Pd NPs, Fig. S4 in the ESM), D is

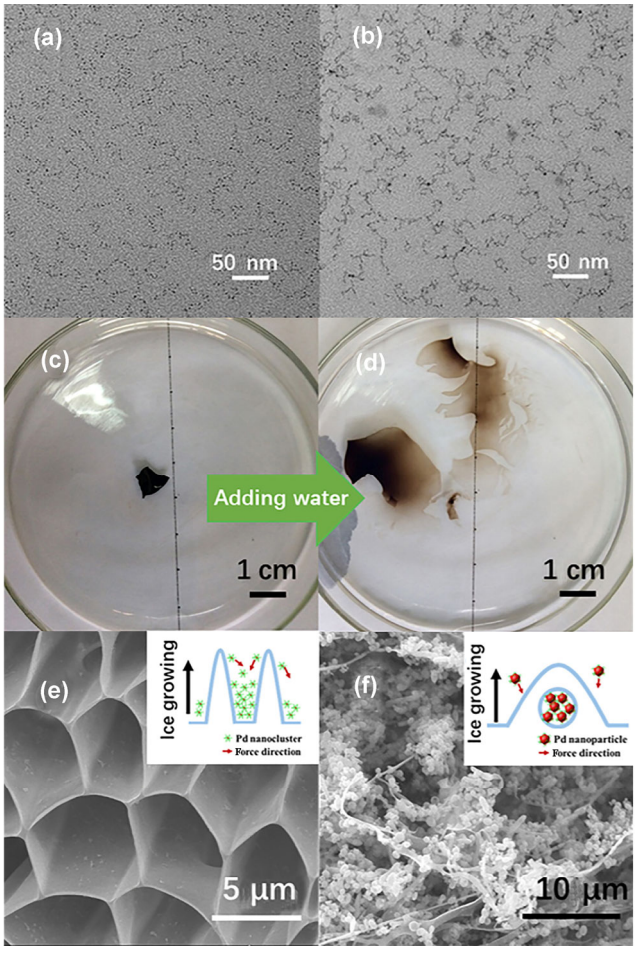

Figure 4 (a) and (b) 1D assembly of Pd NCs. (c) and (d) The bulk Pd NCs can separate to form films on surface of water. (e) and (f) SEM images of PNA1 and freezing Pd nanoparticles about 14 nm in size, both insets are a schematic representation of the ice solidification front.

the distance between the ice front and the Pd NCs or NPs, a_0 is the average intermolecular distance, n refers to a constant between 1 and 4 (2 for Pd NCs, 4 for Pd NPs), $\Delta\sigma$ refers to the balance of the surface forces at the boundary of the ice/particle/solution. v refers to the ice growth velocity, and η is the viscosity of the suspension.

For a typical particle system, when the particle size is decreased, F_r will increase a greater rate than F_a. For 1.8 nm Pd NCs, F_r will lead their movement to escape from the ice solidification front. However, F_a was greater than F_r for the 14 nm Pd NPs and both the values were quite small. Therefore, the Pd NPs were engulfed by ice to form aggregates, which were microspheres in this case.

Further efforts were made to elucidate the assembly of Pd NCs into honeycomb structures that are highly oriented over a large scale and area. This was closely allied to the solidification front velocity for the trapping of Pd nanocrystals, which is given by the following equation [28]

$$v_c = \frac{\rho_l}{9\eta\rho_s}\left[-\frac{A}{2\pi Dd} - gDd(\rho_p - \rho_l)\right] \quad (3)$$

where A is the Hamaker constant, and ρ_p, ρ_s, and ρ_l are the densities of the Pd NCs, solid, and liquid phases. η, D, and d are same as those in Eqs. (1) and (2).

The mathematical treatment of Eq. (3) (for details, see the ESM) revealed that the rate of increase of v_c will be greater upon the decrease of d in the nanoscale range, which can be considered as the size effect.

Therefore, the Pd NCs would need to have a high speed of v_c, in order to escape from the ice solidification front and assemble quickly between the ice columns. In addition, the Pd NCs were uniform and monodisperse to ensure the formation of homogeneous aligned pores over a large area.

To investigate the properties and applications of the Pd NC based assemblages, we carried out room temperature reduction of p-nitrophenol by $NaBH_4$, catalyzed by the assemblages ($NaBH_4$:p-nitrophenol with a molar ratio of 1:1). First, we prepared a piece of hydrophobic treated (for details, see the ESM) PNA1 (h-PNA1, 3.69 mg in this case), fixed it on tweezers, stirred the solution gently, and then took out solution samples every 20 s for testing (10 s for the first point). Figure 5(a) showed the absorbance spectra from 250–500 nm. The decrease of peak intensity at 400 nm and a slightly increase at ~ 320 nm indicated the conversion of p-nitrophenol to p-aminophenol over time. The rate constant for the catalyst was about 0.13 min/mg for h-PNA1, which confirmed the catalytic activity of the materials. We could perform the h-PNA1 (6.70 mg in this case) to the catalytic reaction as a trigger, putting it in or taking it out from catalytic system could realize the switch of the reaction. Thus, the results revealed that the assemblage showed good performance [24, 29, 30].

Palladium is one of the earliest known hydrogen storage materials [31, 32], though it was uneconomical

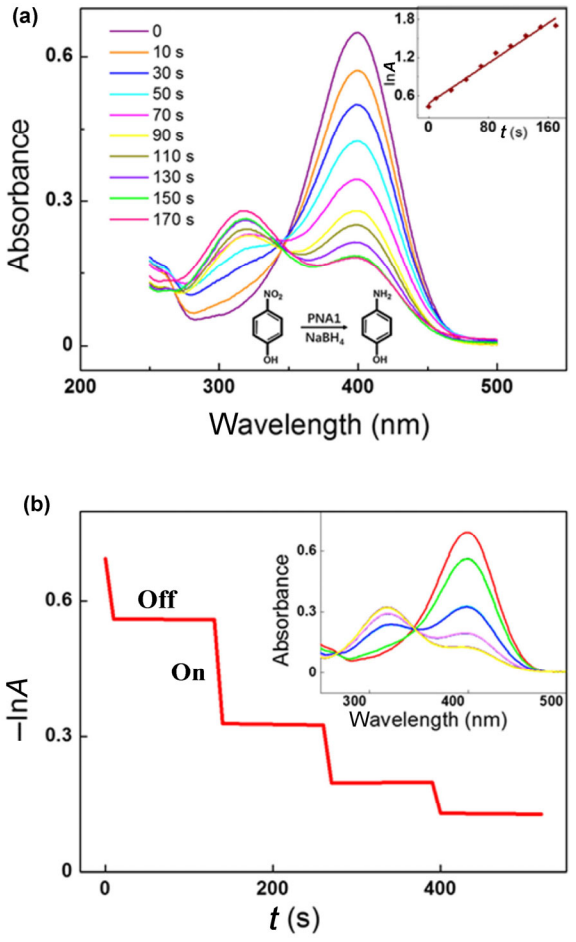

Figure 5 UV–vis spectroscopy monitoring the conversion of p-nitrophenol to p-aminophenol catalyzed by PNA1. (a) The decline of the absorbance spectrum over time as the conversion takes place. The top right inset was the catalytic activity shown as the peak absorbance at 400 nm plotted versus time. (b) Step line as a switch during catalytic process by putting in/taking out PNA1 to control on/off. The inset was the absorbance spectrum over time corresponding to step line.

to use bulk Pd directly. In our case, the Pd NCs were 1.8 nm in size and highly dispersed in oriented structures. We believed that gas phase catalysis based on hydrogen can be carried out in uniform micrometer sized channels in the future. Temperature programmed desorption (TPD) tests were performed to analyze hydrogen desorption from the assemblages in the range 50–250 °C (Fig. S11 in the ESM). The results indicated that a commensurable amount of hydrogen in relation to Pd could be desorbed in a stable state in the assemblages, while PNA1 and PNA2 could desorb hydrogen at a steady rate, which are promising for applications.

4 Conclusion

To conclude, we introduced a highly oriented macroscale honeycomb assemblage based on 1.8 nm Pd NCs. Other assemblages including layered and disordered porous structures were achieved in this system by modulation of the freezing conditions. The size of the building blocks was the key factor for the assembly; we did not obtain ordered assemblages when the 1.8 nm Pd NCs were replaced by 14 nm Pd NPs. The size effect was also manifested in the high escaping speed of the Pd NCs from the ice solidification front to realize multiple assemblies. The energy scale of the building blocks was tailored to keep the assemblage stable. The assemblages based on Pd NCs were found to be effective heterogeneous catalysts for the reduction of p-nitrophenol and as hydrogen storage materials. We believe that the highly oriented assemblages could find application in biomimetics and catalysis.

Acknowledgements

This work was supported by the National Natural Science Foundation of China (NSFC) (Nos. 21431003 and 21521091) and China Ministry of Science and Technology under contract of 2016YFA0202801.

Electronic Supplementary Material: Supplementary material is available in the online version of this article at https://doi.org/10.1007/s12274-017-1723-z.

References

[1] Deville, S. Freeze-casting of porous biomaterials: Structure, properties and opportunities. *Materials* **2010**, *3*, 1913–1927.

[2] Mao, L. B.; Gao, H. L.; Yao, H. B.; Liu, L.; Cölfen, H.; Liu, G.; Chen, S. M.; Li, S. K.; Yan, Y. X.; Liu, Y. Y. et al. Synthetic nacre by predesigned matrix-directed mineralization. *Science* **2016**, *354*, 107–110.

[3] Chen, Y.; Shi, J. L. Mesoporous carbon biomaterials. *Sci. China Mater.* **2015**, *58*, 241–257.

[4] Yang, S. Y.; Ryu, I.; Kim, H. Y.; Kim, J. K.; Jang, S. K.; Russell, T. P. Nanoporous membranes with ultrahigh selectivity and flux for the filtration of viruses. *Adv. Mater.* **2006**, *18*, 709–712.

[5] Gao, H. L.; Zhu, Y. B.; Mao, L. B.; Wang, F. C.; Luo, X. S.; Liu, Y. Y.; Lu, Y.; Pan, Z.; Ge, J.; Shen, W. et al. Super-elastic and fatigue resistant carbon material with lamellar

multi-arch microstructure. *Nat. Commun.* **2016**, *7*, 12920.

[6] Qiu, L.; Liu, J. Z.; Chang, S. L. Y.; Wu, Y. Z.; Li, D. Biomimetic superelastic graphene-based cellular monoliths. *Nat. Commun.* **2012**, *3*, 1241.

[7] Deville, S.; Saiz, E.; Nalla, R. K.; Tomsia, A. P. Freezing as a path to build complex composites. *Science* **2006**, *311*, 515–518.

[8] Yan, F.; Ding, A. L.; Gironès, M.; Lammertink, R. G. H.; Wessling, M.; Börger, L.; Vilsmeier, K.; Goedel, W. A. Hierarchically structured assembly of polymer microsieves, made by a combination of phase separation micromolding and float-casting. *Adv. Mater.* **2012**, *24*, 1551–1557.

[9] Fu, Q.; Rahaman, M. N.; Dogan, F.; Bal, B. S. Freeze casting of porous hydroxyapatite scaffolds. I. Processing and general microstructure. *J. Biomed. Mater. Res. B. Appl. Biomater.* **2008**, *86B*, 125–135.

[10] Li, J. J.; Seok, S. I.; Chu, B. J.; Dogan, F.; Zhang, Q. M.; Wang, Q. Nanocomposites of ferroelectric polymers with TiO_2 nanoparticles exhibiting significantly enhanced electrical energy density. *Adv. Mater.* **2009**, *21*, 217–221.

[11] Han, L. N.; Ye, T. N.; Lv, L. B.; Wang, K. X.; Wei, X.; Li, X. H.; Chen, J. S. Supramolecular nano-assemblies with tailorable surfaces: Recyclable hard templates for engineering hollow nanocatalysts. *Sci. China Mater.* **2014**, *57*, 7–12.

[12] Desvaux, C.; Amiens, C.; Fejes, P.; Renaud, P.; Respaud, M.; Lecante, P.; Snoeck, E.; Chaudret, B. Multimillimetre-large superlattices of air-stable iron-cobalt nanoparticles. *Nat. Mater.* **2005**, *4*, 750–753.

[13] Fu, Q.; Ran, G. J.; Xu, W. L. Direct self-assembly of CTAB-capped Au nanotriangles. *Nano Res.* **2016**, *9*, 3247–3256.

[14] Ni, B.; Wang, X. Chemistry and properties at a sub-nanometer scale. *Chem. Sci.* **2016**, *7*, 3978–3991.

[15] Wang, C. Y.; Siu, C.; Zhang, J.; Fang, J. Y. Understanding the forces acting in self-assembly and the implications for constructing three-dimensional (3D) supercrystals. *Nano Res.* **2015**, *8*, 2445–2466.

[16] Wu, Y. E.; Wang, D. S.; Li, Y. D. Understanding of the major reactions in solution synthesis of functional nano-materials. *Sci. China Mater.* **2016**, *59*, 938–996.

[17] MacLachlan, M. J.; Manners, I.; Ozin, G. A. New(inter) faces: Polymers and inorganic materials. *Adv. Mater.* **2000**, *12*, 675–681.

[18] Gao, H. L.; Xu, L.; Long, F.; Pan, Z.; Du, Y. X.; Lu, Y.; Ge, J.; Yu, S. H. Macroscopic free-standing hierarchical 3D architectures assembled from silver nanowires by ice templating. *Angew. Chem., Int. Ed.* **2014**, *53*, 4561–4566.

[19] Butler, M. F. Instability formation and directional dendritic growth of ice studied by optical interferometry. *Cryst. Growth Des.* **2001**, *1*, 213–223.

[20] Butler, M. F. Growth of solutal ice dendrites studied by optical interferometry. *Cryst. Growth Des.* **2002**, *2*, 59–66.

[21] Butler, M. F. Freeze concentration of solutes at the ice/solution interface studied by optical interferometry. *Cryst. Growth Des.* **2002**, *2*, 541–548.

[22] Deville, S. Freeze-casting of porous ceramics: A review of current achievements and issues. *Adv. Eng. Mater.* **2008**, *10*, 155–169.

[23] Zhang, H. F.; Hussain, I.; Brust, M.; Butler, M. F.; Rannard, S. P.; Cooper, A. I. Aligned two- and three-dimensional structures by directional freezing of polymers and nano-particles. *Nat. Mater.* **2005**, *4*, 787–793.

[24] Nyström, G.; Fernández-Ronco, M. P.; Bolisetty, S.; Mazzotti, M.; Mezzenga, R. Amyloid templated gold aerogels. *Adv. Mater.* **2016**, *28*, 472–478.

[25] Hu, S.; Liu, H. L.; Wang, P. P.; Wang, X. Inorganic nanostructures with sizes down to 1 nm: A macromolecule analogue. *J. Am. Chem. Soc.* **2013**, *135*, 11115–11124.

[26] Xia, B. Y.; Wu, H. B.; Yan, Y.; Lou, X. W.; Wang, X. Ultrathin and ultralong single-crystal platinum nanowire assemblies with highly stable electrocatalytic activity. *J. Am. Chem. Soc.* **2013**, *135*, 9480–9485.

[27] Wang, P. P.; Yang, Y.; Zhuang, J.; Wang, X. Self-adjustable crystalline inorganic nanocoils. *J. Am. Chem. Soc.* **2013**, *135*, 6834–6837.

[28] Li, W. L.; Lu, K.; Walz, J. Y. Freeze casting of porous materials: Review of critical factors in microstructure evolution. *Int. Mater. Rev.* **2012**, *57*, 37–60.

[29] Wang, Q.; Jia, W. J.; Liu, B. C.; Dong, A.; Gong, X.; Li, C. Y.; Jing, P.; Li, Y. J.; Xu, G. R.; Zhang, J. Hierarchical structure based on Pd (Au) nanoparticles grafted onto magnetite cores and double layered shells: Enhanced activity for catalytic applications. *J. Mater. Chem. A* **2013**, *1*, 12732–12741.

[30] Shoaib, A.; Ji, M. W.; Qian, H. M.; Liu, J. J.; Xu, M.; Zhang, J. T. Noble metal nanoclusters and their *in situ* calcination to nanocrystals: Precise control of their size and interface with TiO_2 nanosheets and their versatile catalysis applications. *Nano Res.* **2016**, *9*, 1763–1774.

[31] Higuchi, K.; Yamamoto, K.; Kajioka, H.; Toiyama, K.; Honda, M.; Orimo, S.; Fujii, H. Remarkable hydrogen storage properties in three-layered Pd/Mg/Pd thin films. *J. Alloys Compd.* **2002**, *330–332*, 526–530.

[32] Gu, X. J.; Lu, Z. H.; Jiang, H. L.; Akita, T.; Xu, Q. Synergistic catalysis of metal–organic framework-immobilized Au–Pd nanoparticles in dehydrogenation of formic acid for chemical hydrogen storage. *J. Am. Chem. Soc.* **2011**, *133*, 11822–11825.